Available online at www.sciencedirect.com
SCIENCE DIRECT®
Journal of Nuclear Materials 337–339 (2005) 466–470
journal of nuclear materials
www.elsevier.com/locate/jnucmat

Modeling of three-dimensional neutral transport in tandem mirror plasmas using a Monte-Carlo code

Y. Nakashima [a,*], Y. Higashizono [a], T. Ohki [a], M. Shoji [b], S. Kobayashi [c], Y. Kubota [a], M. Yoshikawa [a], M.K. Islam [a], K. Watanabe [a], T. Ogita [a], M. Yamada [a], R. Murakami [a], T. Cho [a]

[a] *Plasma Research Center, University of Tsukuba, 1-1-1 Tennodai, Tsukuba, Ibaraki 305-8577, Japan*
[b] *National Institute for Fusion Science, 322-6 Oroshi-cho, Toki, Gifu 509-5292, Japan*
[c] *Institute of Advanced Energy, Kyoto University, Gokasho, Uji 611-0011, Japan*

Abstract

Modeling of neutral transport in the tandem mirror plasmas has been performed based on simulation studies using a Monte-Carlo code. A three-dimensional neutral transport simulation in both the central-cell (an axisymmetric simple mirror) and anchor-cell (a non-axisymmetric minimum-B configuration) was successfully carried out using the DEGAS version 63 code. In order to realize the geometrical structure in the simulation space, a 'second wall' is introduced in the code, which enabled us to perform a more detailed simulation. The simulation results agreed well with the Hα measurements of the experiment. The effect of cold gas influx from the beamline of the neutral beam injection (NBI) system on the particle fueling is also investigated and it is found that the azimuthally uniform particle source due to the recycling on the central vacuum chamber wall prevails over the localized fueling from cold gas influx accompanying the NBI.

PACS: 52.25.Ya; 52.40.Hf; 52.55.Jd; 52.65.Pp
Keywords: GAMMA 10; DEGAS; Neutral modeling; Tandem mirror; Hydrogen recycling

1. Introduction

The effect of neutrals on the core plasma performance plays a crucial role in the optimization of the energy confinement and in achieving high-β tandem mirror plasmas as well as tokamak plasmas [1–3]. Particularly in tandem mirror plasmas, penetration of neutrals into the core plasma region plays an important role in formation of the neutral density profile, since the plasma density is lower than that of tokamaks. Neutral particle transport simulations based on the Monte-Carlo methods have been widely used as a standard way to approach neutral behavior in the complicated systems of fusion devices. The modeling of neutral transport using the Eirene [4] and DEGAS2 [5] Monte-Carlo codes is important in the studies of divertor modeling in toroidal systems, such as tokamaks.

In the GAMMA 10 tandem mirror, the neutral transport code DEGAS [6] has been applied and simulation studies have been performed, investigating the neutral

* Corresponding author. Tel.: +81 298 53 7473; fax: +81 298 53 6202.
E-mail address: nakashma@prc.tsukuba.ac.jp (Y. Nakashima).

0022-3115/$ - see front matter
doi:10.1016/j.jnucmat.2004.09.060

particle behavior in tandem mirror plasmas [1,2,7,8]. In the early period of GAMMA 10 research, the neutral density profile in the central-cell has been evaluated by using arrays of Hα detectors axially and radially aligned in conjunction with the above simulation studies [9,10]. Recently neutral beam injection (NBI) experiments have begun in both the central-cell and anchor-cells, which reveal a significant effect on particle fueling in both regions [8,11]. In order to clarify the detailed behavior of neutral particles, a three-dimensional neutral transport simulation is required due to the three-dimensional geometry of the device and the presence of non-axisymmetric sources. In this paper, we describe neutral transport modeling in the non-axisymmetric configuration of GAMMA 10 tandem mirror, using the DEGAS Monte-Carlo code and discuss detailed characteristics of neutral particle sources deduced from the simulations.

2. Model description

2.1. The GAMMA 10 device and experimental systems

GAMMA 10 consists of an axisymmetric central-mirror cell, anchor-cells with a minimum-B configuration using baseball coils, and plug/barrier cells with axisymmetric mirrors [12]. The central-cell, 6 m in length and 1 m in diameter, is connected to the anchor-cells through the mirror throat regions. Initial plasma is produced by two plasma guns from both ends and then the main plasma is built up with ion cyclotron range of frequency (ICRF) waves excited in the central-cell and anchor-cells, respectively. Two gas puffers are installed for sustaining plasma at both mirror throat regions. Neutral beam injectors (NBIs) for heating and fueling the plasma are installed 1.23 m away from the central midplane and at the midplane of both anchor-cells. In the central-cell, an array of five Hα detectors is installed along the machine axis (z-axis) and two radially aligned detector arrays (x, y-direction) are mounted near the midplane. Three other detectors are installed at inner-transition, outer-transition and midplane of the east anchor-cell, respectively. All of the detectors are absolutely calibrated by using a standard lamp. The schematic view of the above diagnostic system and the experimental set-up is shown in Fig. 1.

2.2. Mesh model for the DEGAS code

The three-dimensional neutral transport simulation has been performed by using the DEGAS ver.63 Monte-Carlo code [13]. In this code the modifications of atomic-molecular interactions, such as dissociative–excitation reactions, are introduced in the dissociation energy and reaction rates, which becomes significant at lower densities [1]. Fig. 1 shows the mesh model of the

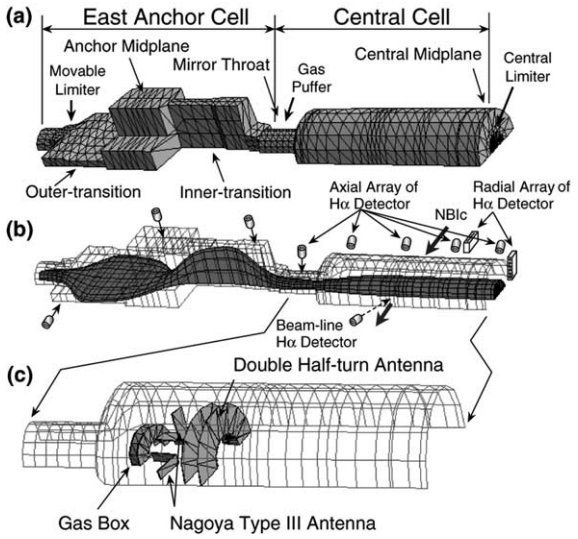

Fig. 1. Mesh model used for the 3D-DEGAS simulation. (a) surface structure of the vessel wall, (b) grid shape of the plasma surface, and (c) structure of the 'second wall' introduced into the code.

wall surface of the vacuum chamber in the central and anchor cells, together with the grid structure of the plasma surface and the components installed in the vacuum chamber used in the present calculation. In this model, as shown in the figure, an up–down symmetry is introduced and the simulation space is divided into 11 segments radially and 8 segments azimuthally. In the axial direction, 69 segments are defined, which extend from the central midplane to the outer-transition of the anchor-cell. In order to apply the geometrical structure precisely into the simulation space, additional structures, 'second wall', are defined. In the present simulation, a gasbox and two ICRF antennas are treated as isolated walls in addition to the 3-dimensional mesh structure of the central-cell vacuum vessel wall. The components defined as the second wall are shown in Fig. 1(c). After introducing this boundary condition, a modification of the algorithm has been made in the code, which preserves the consistency in particle tracking with interactions between test particles and the 'second wall'.

2.3. Modeling of plasma parameters and particle sources

Fig. 2(a) shows the plasma parameter model adopted in the simulation. In the density model, particle flux conservation of the flowing plasma is assumed along the axial direction. Then the density profile is determined on the basis of the measured data at the central-cell, the mirror throat and the anchor midplane, considering the shape of the magnetic flux tube. The parallel ion

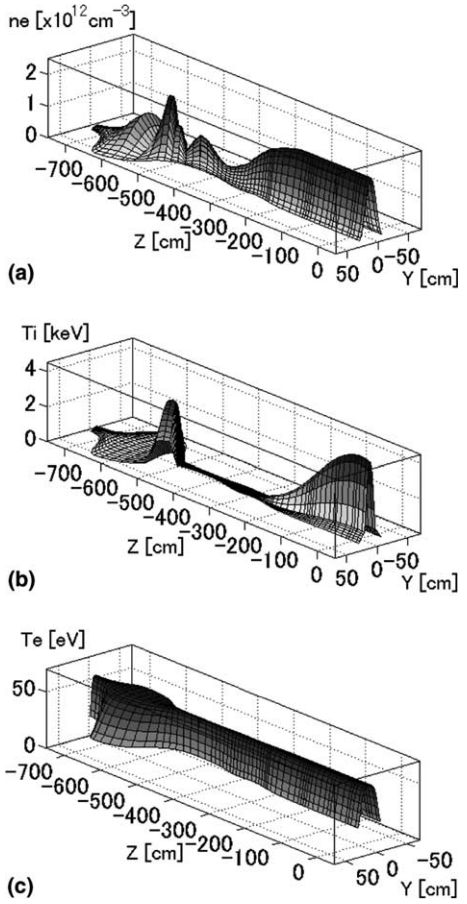

Fig. 2. Spatial profiles (in the y–z plane) of plasma parameters used in the simulation. (a) n_e, (b) T_i, and (c) T_e.

velocity is determined from $T_{i\parallel}$ measured with the end-loss ion energy analyzer. The ion temperature profile is shown in Fig. 2(b). The radial profile is determined using a charge-exchange neutral particle analyzer, and its axial variation is obtained from axial distribution of the diamagnetic signals in the central-cell. The electron temperature profile is taken to be constant along the magnetic flux tube based on the soft X-ray measurements. In the plasma shot used in the present simulation, NBI was carried out only in the central-cell. Therefore, the following particle sources are given in the simulation; (a) gas influx from a gas puffer near the mirror throat, (b) hydrogen recycling near the central midplane, (c) hydrogen recycling at a movable limiter inserted in the outer-transition of the anchor-cell and (d) gas influx from the beam line of the central-cell NBI. The calculated neutral density is converted to Hα emissivity along the sight line of each detector on the basis of the collisional-radiative model [14] that includes the effects of molecular dissociation processes. Obtained results are normalized by optimizing the intensity of each particle source individually so as to fit to the experimental results at every measured position. In this way the most plausible neutral density profiles are determined.

3. Results and discussion

3.1. Spatial profile of neutral hydrogen density

The simulation results are shown in Fig. 3. In this simulation, three particle sources (from the gas puffer at the mirror throat, from hydrogen recycling at the central midplane and from the movable limiter at the outer-transition region) are considered. The portion of each particle source rate is 6.2, 1.4 and 0.15, respectively in relative units. As shown in Fig. 3(b), atomic hydrogen density has a peak value at the mirror throat and is reduced by two order of magnitude toward the central midplane (-300 cm $\leqslant z \leqslant -150$ cm) in the plasma edge region, since the components, such as the ICRF antennas and the gasbox, prevent neutral transport in the vacuum chamber. The atomic density ceases to decrease at $z = -150$ cm due to the enhancement of hydrogen recycling near the midplane where hot ions are produced by

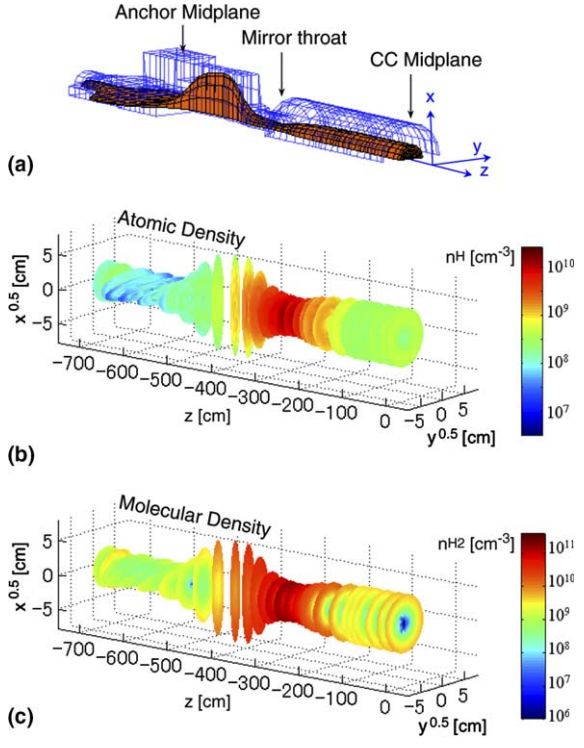

Fig. 3. Results of the 3D-DEGAS simulation. (a) mesh of the wall and plasma surface, (b) atomic hydrogen density, and (c) molecular hydrogen density. The x and y axes are reduced to a square-root scale.

strong ICRF heating ($-150\ \text{cm} \leqslant z \leqslant +150\ \text{cm}$) [2]. In the anchor-cell, on the other hand, a strong reduction of the neutral density is observed through the inner-transition region where the plasma cross-section becomes very flat. Beyond that, the density increases slightly owing to recombined hydrogen on the movable limiter at the outer-transition. Molecular hydrogen density shown in Fig. 3(c) exhibits the similar characteristics in spatial profiles.

The above results qualitatively agree with those of an axisymmetric simulation previously carried out in the central-cell [2,7] as well as a preliminary 3-d simulation performed only in the anchor-cell [8,15]. Consequently the present simulation is thought to be consistently performed by using the DEGAS ver.63 code in the region from the central midplane to the outer-transition of the anchor-cell.

3.2. Comparison between simulation and measurement

From the above calculated neutral density profiles, Hα emissivity in each mesh element is determined and is integrated along the actual sight line of each detector. Fig. 4 shows the comparison between the simulation results and the measurements in the central-cell. The open circles in the figure represent the Hα intensities determined from the simulation in which only the central-cell is modeled and a simple exit is located at the outside of the mirror throat. In this case, it should be noted that a discrepancy is observed at the location of the gasbox ($z = -240$ cm). This result indicates that a significant fraction of particles reflected at the sidewall of the gasbox is lost toward the exit that is defined in place of the connecting region to the anchor-cell. This leads to the reduction of neutral density at the gasbox. However, the triangles obtained from the present simulation, in which both central-cell and anchor-cell are combined into one structure, reproduces well the experimental results (shown as filled circles). On the other hand, the data represented by crosses are obtained from another simulation in which the thickness of the gasbox is artificially reduced by half in axial direction. In this case, a noticeably higher intensity of calculated Hα emission is seen. From these results, it is clear that the neutral transport is much affected by a geometrical configuration in the mirror throat region, which also points out the importance of the second wall in the simulation.

3.3. Effect of gas influx from the NBI in the central-cell

Fig. 5 is an example showing the effect of non-uniform particle source on the neutral density profile in the central-cell. Here a particle source rate of 1.58 (in the same relative units used in Section 3.1) is applied at the location of the NBI injection port in order to simulate only the cold gas influx from the beam line of the NBI. As shown in the figure, a strong localization of neutral density is observed in front of the injection port ($z = -120$ cm). This localization in neutral density is dispersed with the distance from the beam line and becomes almost axisymmetric 50 cm away from the injection port ($z = -70$ cm), which is consistent with the measured results from the nearest radial Hα detector array ($z = -52$ cm). In order to clarify the physical mechanism of this dispersal of neutrals, further experiments and simulations are necessary. However, the

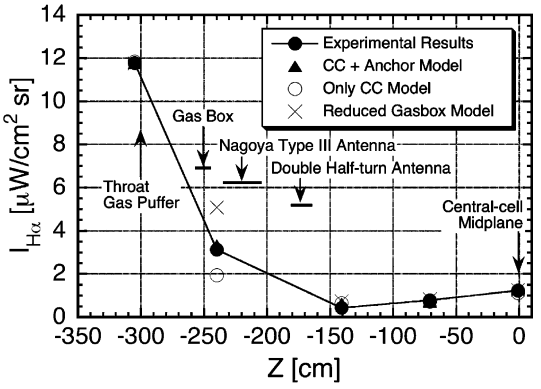

Fig. 4. Axial intensity profile of Hα line-emission. The solid circles are the experimental results. Triangles are the results of the present simulation. Open circles are determined from the simulation without the anchor-cell. Another simulation having a gasbox model of reduced size is shown by crosses.

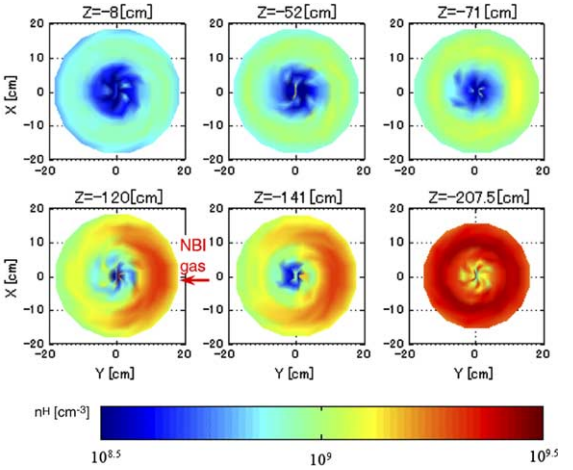

Fig. 5. Spatial profiles (in the x–y plane) of the atomic hydrogen density at different z locations of the central-cell in the case of the simulation of the cold gas influx from the NBI beamline.

above result indicates that an axisymmetric particle fueling due to hydrogen recycling prevails over the localized effects of NBI near the midplane region.

4. Summary

Modeling of neutral transport over the region from the central-cell to the anchor-cell of GAMMA 10 was performed for the first time. Use of a 'second wall' was successfully applied in addition to the usual vacuum chamber wall. It enabled us to realize a detailed three-dimensional particle simulation including complicated structures in the simulation space. A combination of three different particle sources defined at the mirror throat, the central midplane and the movable limiter of the outer-transition lead to better agreement with the experimental results than those of the previous simulation. Neutral particle behavior near the mirror throat is strongly affected by the geometrical configuration of the components installed in the vacuum chamber. A 3-d simulation using non-uniform particle source, such as the cold gas influx from the beamline of the NBI was performed, and it was found that the effect of that cold gas influx is limited to the vicinity of the injection port. The above results may provide useful information for understanding the detailed neutral transport in the complicated structure in the near future plasma devices.

Acknowledgments

The authors would like to acknowledge the members of the GAMMA 10 group, University of Tsukuba for their collaboration in the experiments.

References

[1] Y. Nakashima et al., J. Nucl. Mater. 196–198 (1992) 493.
[2] Y. Nakashima et al., J. Nucl. Mater. 241–243 (1997) 1011.
[3] S.A. Allen et al., Nucl. Fus. 27 (1987) 2139.
[4] D. Reiter et al., Plasma Phys. Contrib. Fus. 33 (13) (1991) 1579.
[5] D.P. Stotler et al., Contrib. Plasma Phys. 34 (1994) 392.
[6] D. Heifetz, D. Post, M. Petravic, et al., J. Comput. Phys. 46 (1982) 309.
[7] S. Kobayashi et al., J. Nucl. Mater. 266–269 (1999) 566.
[8] Y. Nakashima et al., J. Nucl. Mater. 313–316 (2003) 553.
[9] N. Yamaguchi et al., In: Proc. 15th European Conf. Control. Fus. Plasma Heating, Dubrovnik, 16–20 May 1988, vol. 12B, part-II, p. 593.
[10] M. Yoshikawa et al., Trans. Fus. Technol. 35 (1999) 273.
[11] Y. Nakashima et al., Trans. Fus. Sci. Technol. 43 (1T) (2003) 135.
[12] M. Inutake et al., Phys. Rev. Lett. 55 (1985) 939.
[13] D.P. Stotler et al., Phys. Plasmas 3 (1996) 4084.
[14] L.C. Johnson, E. Hinnov, J. Quant. Spectrosc. Radiat. Transfer. 13 (1973) 333.
[15] Y. Nakashima et al., J. Plasma Fus. Res. SERIES 6, (2004), in press.